

Article

Not peer-reviewed version

---

# Consideration of Correlations in Radiometric Measurements of the Environment

---

[Steven W. Brown](#)<sup>\*</sup>, Maritoni A. Litorja, Julia K. Marrs, [David W. Allen](#)

Posted Date: 28 February 2026

doi: 10.20944/preprints202602.2009.v1

Keywords: correlations; covariance; reflectance; uncertainties; vicarious calibration



Preprints.org is a free multidisciplinary platform providing preprint service that is dedicated to making early versions of research outputs permanently available and citable. Preprints posted at Preprints.org appear in Web of Science, Crossref, Google Scholar, Scilit, Europe PMC.

Copyright: This open access article is published under a [Creative Commons CC BY 4.0 license](#), which permit the free download, distribution, and reuse, provided that the author and preprint are cited in any reuse.

Disclaimer/Publisher's Note: The statements, opinions, and data contained in all publications are solely those of the individual author(s) and contributor(s) and not of MDPI and/or the editor(s). MDPI and/or the editor(s) disclaim responsibility for any injury to people or property resulting from any ideas, methods, instructions, or products referred to in the content.

Article

# Consideration of Correlations in Radiometric Measurements of the Environment

Steven W. Brown \*, Maritoni A. Litorja, Julia K. Marrs and David W. Allen

National Institute of Standards and Technology, Gaithersburg, MD USA

\* Correspondence: swbrown@nist.gov; Tel.: +1 301.975.52167

## Highlights

When making optical measurements in the environment, illumination conditions vary due to fluctuating atmospheric conditions such as turbulence. Understanding the timescales of illumination variations in ratios of measurements between two instruments is important for applications like vicarious calibration of sensors on satellites. In this work, we introduce a multiple-input, fiber-coupled spectrograph that enables multiple measurements from disparate targets to be acquired simultaneously. Using this instrument, a metric toward furthering understanding of covariance timescales of two environmental measurements is developed. Results presented in this work may positively influence data acquisition protocols in situations with unstable illumination sources, with environmental measurements being a prime example.

## Abstract

Vicarious calibration is a technique that makes use of radiometrically stable targets such as high-altitude dry lakebeds and north African desert sites for the post-launch calibration of a satellite sensor. Top-of-the-atmosphere radiances or reflectances are provided for the calibration of the sensor. The reflectance of a remote sensing vicarious calibration site is measured by ratioing the signal from a ground target to the signal from a reference artifact whose reflectance is known. There can be elapsed times between measurements of a reference artifact on the order of 10 min. For environmental measurements, the solar illumination can vary on time scales relevant to the delay between measurements of a target and a reference artifact, impacting the variance in the measured reflectance. In this work, we explore the impact of a temporal delay between two measurements taken outdoors on the Type A uncertainties in their ratios. A factor of 3 reduction in the Coefficient of Variation of the ratio taken simultaneously versus sequentially with delays on the order of 10 min was realized. Implications for protocols employed to measure the surface reflectance at sites used for the vicarious calibration of aircraft and satellite sensors are discussed.

**Keywords:** correlations; covariance; reflectance; uncertainties; vicarious calibration

---

## 1. Introduction

Sensors on satellites are used to make regional and global measurements of optical properties of land, water, and atmosphere, providing information about the state of the Earth's biosphere. Sensor responsivities can change due to vibrations during launch and the harsh environment of space once on-orbit. Monitoring changes in a sensor's response and validating its performance over its mission lifetime is required to properly understand uncertainties in measurements by the space-borne sensor and uncertainties in data products derived from those measurements [1]. Calibration methodologies that are not onboard the sensor platform [2], commonly referred to as vicarious calibrations, have historically been, and continue to be, an essential component of post-launch operational protocols [3,4]. Use of Pseudo-Invariant Calibration Sites like those sites that are a part of the Radiometric Calibration Network (RadCalNet) continues to be a staple of vicarious calibration strategies [5–10].

RadCalNet provides SI-traceable Top-of-Atmosphere (TOA) spectrally-resolved reflectances at 4 different sites to aid in the post-launch radiometric calibration and validation of optical imaging sensors.

For vicarious calibration, the top-of-the-atmosphere reflectance or radiance from a vicarious calibration target, measured as closely as possible to the time of a satellite overflight, is provided to the sensor team. *in situ* measurements by onsite personnel remains a common approach to characterize a land vicarious calibration site. To obtain the reflectance of the test site, a researcher walks a defined pattern with an instrument, measuring the site reflectance frequently, and returning occasionally to measure the reflectance of a reference panel. In this manner, measurements of some fraction of the size of a region of several pixels in a satellite sensor image are made close in time to a sensor overflight. In the case of Landsat 7, Ground Sampling Distance of 30 m, for example, the Railroad Valley vicarious calibration site [5,11] was mapped over a rectangular area of 420 m by 120 m [12]. A team member walked a path parallel to the cross-track direction of Landsat 7 through the center of 4 cross-track pixels for all 16 along-track pixels. Approximately 640 samples taken over approximately 2.5% of the site area were used to represent the entire area. It took 45 min to 60 min to collect the data set; measurements of the reference reflectance panel were made at the start and end of the data collection, as well as every 80 test-site samples, or approximately every 5 min to 10 min. The uncertainty in spectral reflectance measurements at Railroad Valley taken on June 1, 1999, is approx. 2% from 400 nm to 1800 nm, increasing to 4% in shorter (400 nm to 300 nm) and longer (2000 nm to 2400 nm) wavelength regions [12,13]. These are typical uncertainties in ground reflectance measurements at vicarious calibration sites [14]. There are several additional uncertainty components in the TOA reflectance such as site inhomogeneity and atmospheric transmittance [12]. Uncertainties in measurements of ground reflectance contribute significantly to the uncertainty in the TOA reflectance provided to a sensor team.

This leads to consideration of measurement approaches to reduce the uncertainty in environmental reflectance measurements. The propagation of a light beam through the atmosphere is affected by random fluctuations in ozone concentration, water vapor concentration, and in the refractive index of air, also known as turbulence, resulting in a spatially and temporally variant light field at the surface [15,16]. Consequently, there are both spatial and temporal correlations in environmental measurements; this work focuses on consideration of temporal correlations.

Correlations is a statistical concept that describes the covariance between two variables. Previous work considered correlations in water-leaving radiance, the primary data product used to vicariously calibrate satellite sensor ocean color instruments [17,18]. Historically, the National Oceanic and Atmospheric Administration's (NOAA's) vicarious calibration observatory, the Marine Optical Buoy [17], measured the up-welling radiance from 3 arms located at different depths in the ocean. From these measurements, the water-leaving radiance was determined by propagating the up-welling radiance measurements to the surface and through the water-air interface. Measurements from the 3 buoy arms were acquired sequentially and took about 20 min to complete.

Yarbrough *et al.* [19] considered the impact of temporal correlations on uncertainties in water-leaving radiance. They used a multiple-input, fiber-coupled (MIFC) spectrograph integrated with a small buoy for *in situ* simultaneous measurements of upwelling radiance from multiple independent inputs. In-water measurements acquired simultaneously by the system demonstrated that the Type A uncertainties in the water-leaving radiance can be reduced over sequential measurements by the same system separated by a minute. The magnitude of the reduction was a factor of five in the spectral region between 400 nm and 500 nm, a factor of 3 around 550 nm, and a factor of 2 between 650 nm and 700 nm. The results suggest that, by taking advantage of correlations in the light field, thereby reducing the uncertainty in water-leaving radiance, it may be possible to determine an ocean color satellite sensor's gain using fewer measurements over a much shorter time scale than has been historically required [20].

The spectral dependence on the reduction in the uncertainty in water-leaving radiance for simultaneous measurements observed by Yarbrough *et al.* may be an example of the effect of spatial

correlations on the measurements. The different arms in the water-leaving radiance experiment were located at different depths in the ocean and looked at the up-welling radiance from different paths. Spectral correlations in the temporal evolution of ratios between fiber inputs on different arms of the buoy were modified by the changing spectral scattering length of light in the water. The reduction in the scattering length at longer wavelengths resulted in a decreased spatial correlation between the measurements and contributed to the increased variance observed in the temporal measurements. The water-leaving radiance is a factor of 5 lower at 700 nm than at 475 nm and signal-to-noise may have contributed to the increased variance at longer wavelengths as well.

In this work, we consider the impact of temporal correlations on the uncertainty in ratios of environmental measurements between two input channels of a MIFC spectrograph. The two channels were oriented perpendicular to the plane of two reference reflectance targets separated by 15 cm. Data sets were acquired by measuring the ratio of the signal from Channel 1 (Ch1) measured at a time  $t_0$ ,  $\langle I_1(t_0) \rangle$  to the signal from Channel 2 (Ch2) measured at a time  $t_0 + n_i \cdot \tau$ ,  $\langle I_2(t_0 + n_i \cdot \tau) \rangle$ , normalized by the ratio at time  $t_0$ ,  $\langle I_1(t_0)/I_2(t_0) \rangle$ . The brackets reflect the averaging time of the measurement, *e.g.* the integration time of the camera. The start time of a data set is set to 0.  $\tau$  is the delay between measurements and  $n_i$  varies from 1 to  $n$ , the number of samples in a data set. The normalized ratio is then given by Eq. 1,

$$r_{n_i}(n_i \cdot \tau) = \langle I_1(0)/I_2(n_i \cdot \Delta\tau) \rangle / \langle I_1(0)/I_2(0) \rangle \quad (1)$$

Multiple data sets were acquired,  $j = 1, \dots, N$ , and data were analyzed for each delay  $n_i \cdot \Delta\tau$  using the percent Coefficient of Variation (CoV), defined as 100 times the ratio of the standard deviation to the mean of the multiple data sets,

$$CoV = 100 \cdot \sigma / \mu \quad (2)$$

The experimental setup is described in Section 2; the acquired data sets are described in Section 3 and reduced in Section 4. Section 5 gives a discussion of the results. Conclusions are given in Section 6.

## 2. Materials and Methods

The MIFC spectrograph was developed by Moss Landing Marine Laboratories (MLML) [21]. Characteristics of the spectrograph are given in Table 1. The MLML MIFC spectrograph was a custom Resonon\* prism-grating-prism spectrograph with a Princeton Instruments cooled PIXIS CCD detector. Fourteen, 800 mm core diameter fibers in a RoMack fiber bundle were end-coupled along the length of the entrance slit of the spectrograph. Figure 1a is a picture showing the RoMack fiber bundle input to the in-line Resonon spectrograph with a cooled Princeton Instruments camera at the focal plane. Figure 1b shows the image of the entrance slit on the camera when all 14 fiber inputs are looking at the output from a lamp-illuminated integrating sphere. Colors in the image reflect the magnitude of the raw digital number (DN) from the CCD. Yellow reflects greater DN while blue reflects lower DN. Images of the fibers are approximately 50 pixels wide on the focal plane with approximately 10 pixels between channels. Fiber inputs 5 (Ch1) and 10 (Ch2) were used for the environmental tests.

A camera image of the two input fibers at the spectrograph focal plane looking at the output from a lamp-illuminated integrating sphere is shown in Figure 2a. A cross-sectional view of the intensity profile of the spatial image is shown in Figure 2b. The images reflect a combination of core and cladding modes excited in the optical fiber. Cladding modes give rise to the sharp peaks at the edges of each channel. Signals from the 2 channels were averaged over the spatial regions given by the dashed lines in Fig. 3.

Ratios between 5 spectral bands that approximated NOAA's Visible Infrared Imaging Radiometer Suite (VIIRS) bands M1 through M5 were considered. Bands 1 through 5 are given in Table 2 along with their VIIRS band counterpart. The typical relative signal observed as a function of

wavelength is shown in Figure 4. The grey columns reflect the spectral windows used for bands 1 through 5. Note that bands 1 through 4 have similar signal strengths while the signal from band 5 is reduced by approximately 55%.

**Table 1.** Details of the MLML MIFC spectrograph [1].

Parameter	Value(s)
Spectral range	370 nm to 720 nm
Spectral resolution	Approx. 1 nm
Pixel-to-Pixel spacing	0.33 nm
Slit dimensions	13 mm x 25 $\mu$ m
Image size at focal plane	13 mm x 13 mm

**Table 2.** Spectrograph bands used in the experiment.

VIIRS Band	Band	Center wavelength [nm]	Bandwidth [nm]
M1	1	415	20
M2	2	445	20
M3	3	490	20
M4	4	555	20
M5	5	673	20

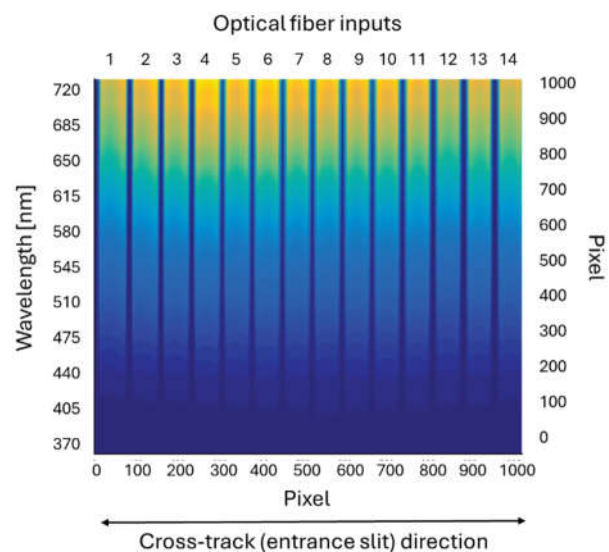
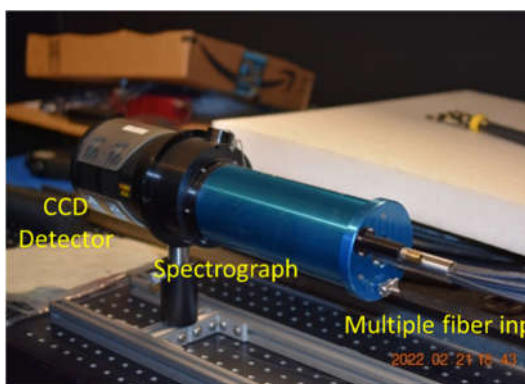


**Figure 1a.** Picture of the MLML MIFC instrument used for this experiment showing the RoMack multiple fiber bundle coupled to the in-line Resonon spectrograph with a cooled Princeton Instruments camera at the focal plane.

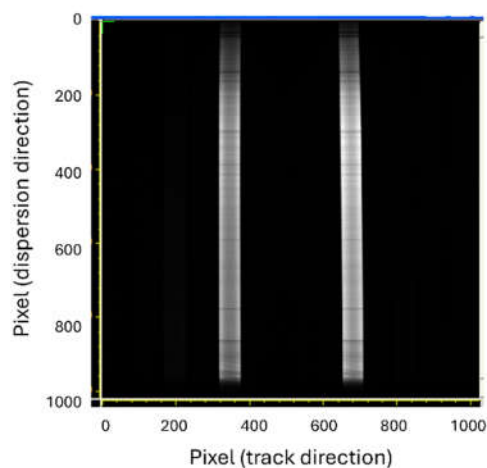


**Figure 1b.** Image on the detector array obtained when all fibers are illuminated uniformly. Colors reflect raw DN, with yellow reflecting larger DN and blue lower DN. (Image provided by Mark Yarbrough, Moss Landing Marine Laboratories.)

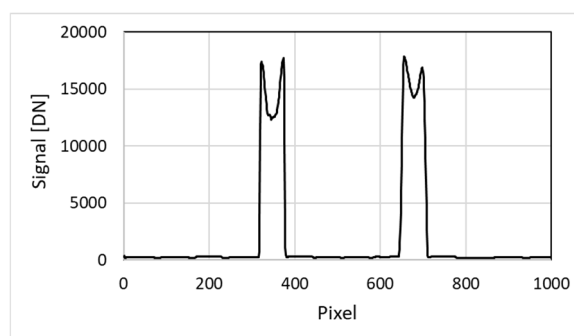


**Figure 2a.** An image of the two input fibers looking at the output from a lamp-illuminated integrating sphere. Relative intensity (DN) is given by the brightness of each pixel.

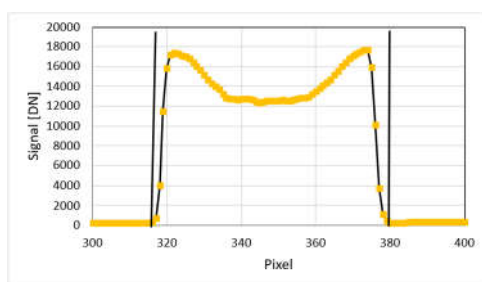


**Figure 3a.** Expanded views of the spatial cross-sections of Ch 1. The dashed lines give the limits used to calculate the average signals.

### 3. Results

Results are divided in a section on the data sets acquired and the data reduction protocols.

#### 3.1. Data Sets

50-mm diameter lenses with 100 cm focal lengths were used to couple incident solar irradiance scattered off 50 mm diameter Avian Technologies reflectance 'pucks' into the optical fibers. Data were acquired in a 15° off-nadir configuration with both radiance heads looking at a common reflectance

**Figure 2b.** Cross-sectional view of the intensity profile of the spatial image averaged over the full spectral profile.

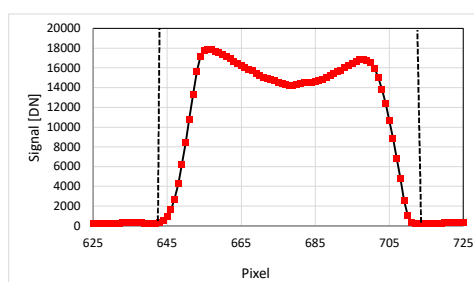


**Figure 3b.** Expanded views of the spatial cross-sections of Ch 2. The dashed lines give the limits used to calculate the average signals.

puck, and a nadir configuration with the 2 channels looking at individual pucks with 2% (Ch1) and 5% (Ch2) reflectance, respectively. The two channels were aligned to the pucks in the laboratory prior to the experiment by backfilling the input heads with a fiber-coupled white LED source and visually aligning the outputs to the center of their reflectance pucks.

The total measurement time for each data collect, 15 min to 20 min, was based on the time between repeat measurements of a reference reflectance panel during Landsat 7 vicarious calibration activities (5 min to 10 min). Two data sets were acquired. For data set 1, 4 repeat data collects were acquired every 30 s. Data set 2 repeated the collects of data set 1, with data acquired every 15 s.

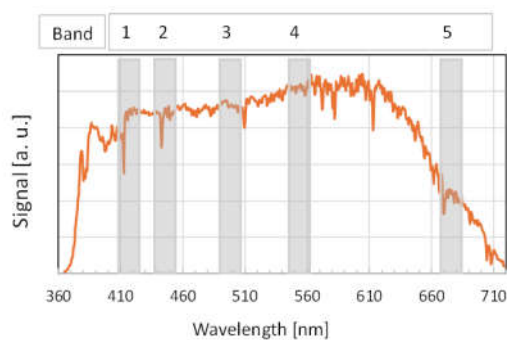


**Figure 4.** Relative spectral distributions measured by the two channels, orange line. The bands evaluated in this work are given by the grey rectangles and are labelled at the top of the figure.

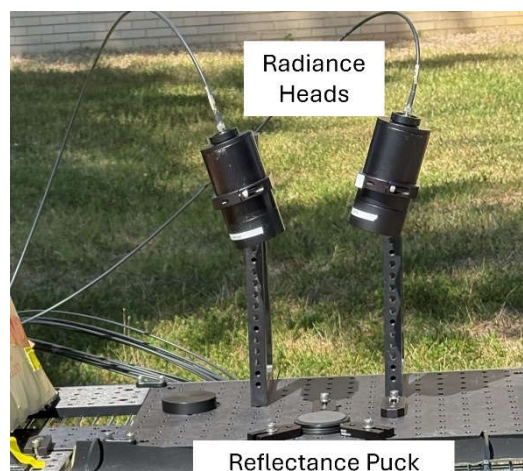


**Figure 5.** Picture of off-nadir setup.

### 3.2. Data Reduction Protocols

The two data sets, separated by a day and taken in the morning and afternoon, respectively, showed very similar results, implying the atmospheric conditions were very similar on the two days. Results from the first data set are presented. Figure 6 shows the CoV of Ch1 to Ch2 band ratios for the 4 data sets with no time delay between measurements (1-1: Ch1 band 1 to Ch2 band 1; 1-2: Ch1 band 1 to Ch2 band 2, etc.). No clear dependence on band ratio was observed. The mean CoV for the 4 data sets, all bands, was taken as the baseline CoV for the band-ratio measurements. The mean CoV is  $0.39\% \pm 0.7\%$ .

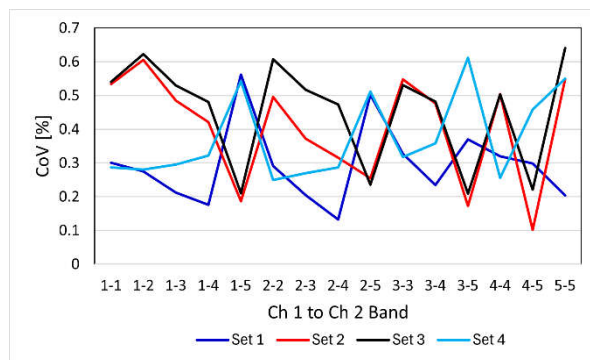


**Figure 6.** CoV of Ch1 to Ch2 band ratios with no time delay between measurements. X-axis labels represent different band ratios. For example, label 1-1 refers to Ch1 band 1 ratioed to Ch2 band 1. The 4 different data collects, Sets 1 through 4, are shown.

Figure 7 shows the CoVs of the 4 repeat data collects for Ch1 ratios between bands, Figure 7a, and Ch2 ratios between bands, Figure 7b, respectively. Band 1 to band x ratios are plotted as a function of elapsed time between measurements. Ch2 looked at the 5% reflectance puck and the signal was 2.5 times greater than the signal from Ch1, that looked at at looked at the 2% reflectance puck. The mean CoV of Ch1 band ratios between band 1 and bands 1-4 is  $0.88\% \pm 0.11\%$ ; the mean CoV of Ch2 band ratios between band 1 and bands 1-4 is  $0.54\% \pm 0.11\%$ . The CoV of the Ch1 band 1 to Ch1 band 5 ratio is larger than the CoV of the other band ratios,  $2.07\% \pm 0.44\%$ ; similarly, the COV of the Ch2 band 1 to Ch2 band 5 ratio is also larger than the CoVs of other band ratios,  $2.17\% \pm 0.43\%$ .

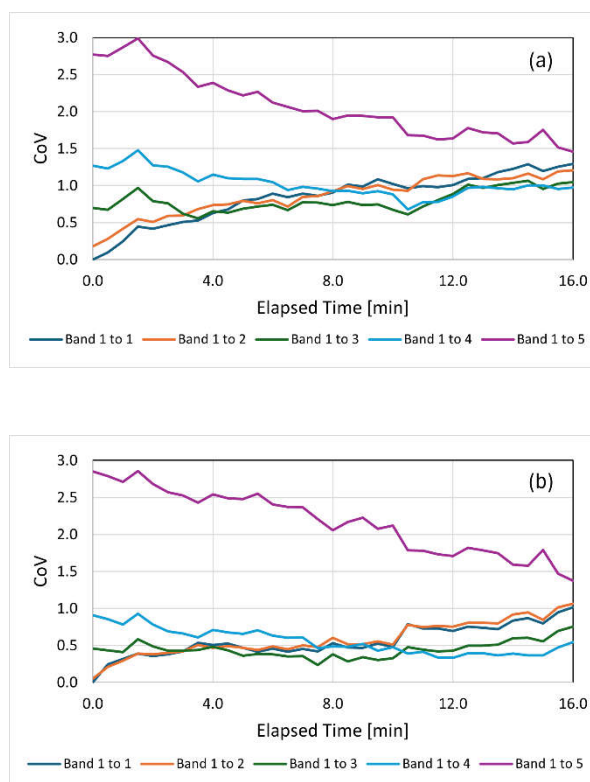


**Figure 7. a).** CoV's Ch1 band 1 to Ch1 band x ratios as a function of elapsed time; **(b).** CoV's of Ch2 band 1 to Ch2 band x ratios as a function of elapsed time. The legend nomenclature, Band 1 to 1, refers to Ch1 band 1 to Ch1 band 1 ratio, etc.

The mean CoV from Ch2 is 60% of the mean CoV from Ch1. The band 1 to band 5 CoV was the same for both channels within their uncertainties. One interpretation of these results is COV's in band

ratios from Ch1 and Ch2 are correlated and the CoV is related to the signal from the two channels whereas the band 1 to band 5 ratio is not as highly correlated and may be determined primarily by the uncertainty in the band 5 signal.

Figure. 8 shows the CoV's of Ch1 band x to Ch2 band y ratios. All band ratios show a linear increase in their CoV as a function of time between the two measurements. The mean CoV for the ratio between Ch1 band 1 and Ch2 bands 1 through 4 for a time difference of 16 min is 1.45 %. The CoV for Ch1 band x to Ch2 band 5 is greatest for all bands, with a mean value of 2.16% for a 16 min time difference between the two measurements.

#### 4. Discussion

Table 3 shows the Ch1 Band 1 ratio to Ch2 Bands 1 through 5 for a time interval between measurements of 0.5 min, 5 min, and 10 min. The results show a factor of 2 to 3 reduction in the CoV when the two data channels are acquired simultaneously versus the situation where two data channels were acquired with a delay of 10 min between measurements. Using these results as a proxy for measurement conditions at different land vicarious calibration sites, acquiring the reflectances of the target (e.g. a dry lakebed) and the reference panel simultaneously may reduce the Type A contribution to the uncertainty budget by a factor of 2 to 3. An examination of the top-of-the-atmosphere reflectance uncertainty budget to evaluate the impact of the reduction in Type A uncertainty in measured reflectance on the uncertainty in the TOA reflectance, while important, is beyond the scope of this work.

Though a multiple-input, fiber-coupled spectrograph was used in the experiments described herein, single channel spectrographs are most commonly used to make hyperspectral measurements of a land site. Consequently, a natural extension of this work is to consider acquisition by two instruments using a common trigger or a reference timing signal. Additionally, using a reference timing signal rather than a common trigger would enable the two acquisition systems to be fully separated from one another and may lead to additional applications, for example simultaneous measurements between a sensor mounted on an aircraft or drone and measurements on the ground.

**Table 3.** the Ch1 Band 1 ratio to Ch2 Bands 1 through 5 for a time interval between measurements of 0.5 min, 5 min, and 10 min.

Band Ratio	CoV [%]		
	Delay between measurements [min]		
	0.5	5	10
1-1	0.24	0.64	0.76
1-2	0.27	0.7	0.81
1-3	0.35	0.76	0.95
1-4	0.53	0.98	1.18
1-5	0.59	1.24	1.59

Simultaneous measurements have been shown to reduce the uncertainties in other optical measurements as well. Using simultaneous measurements during detector calibrations on the Visible near-infrared Spectral Comparator Facility at the National Institute of Standards and Technology (NIST) reduced the uncertainty in the measurement by of 2 orders of magnitude [22].

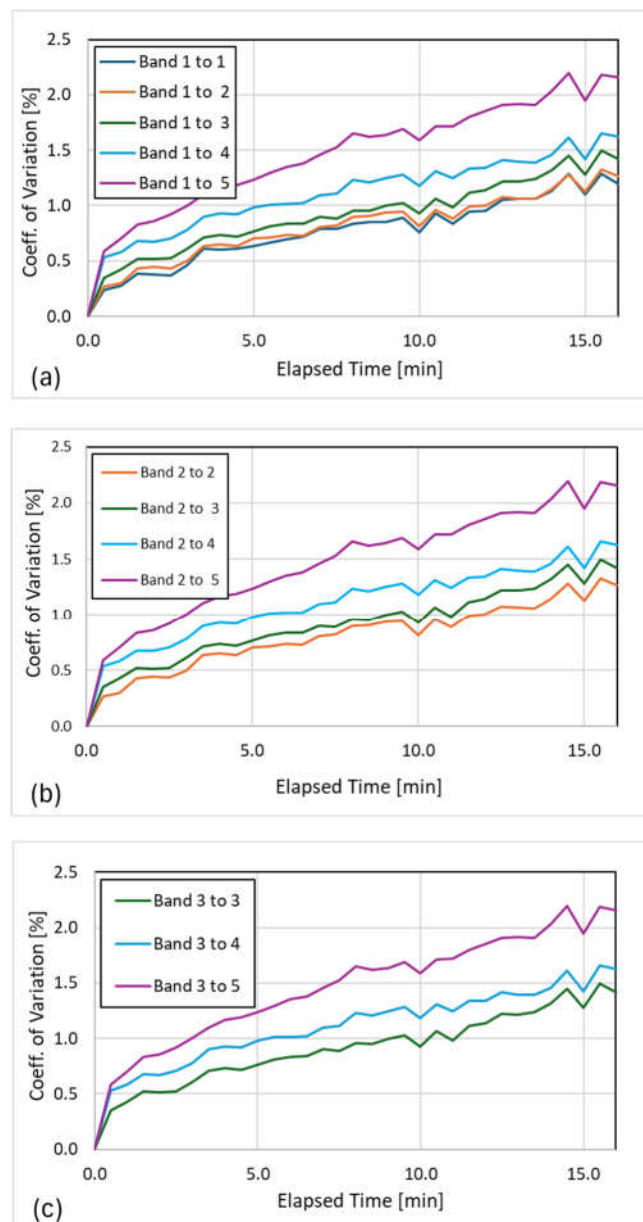


**Figure 8.** CoV's of Ch1 band  $x$  to Ch2 band  $y$  ratios. The legend reflects this. For example, the legend Band 1 to 1 term refers to the Ch1 band 1 to Ch2 band 2 ratio, etc.

## 5. Conclusions

The measurements presented in this work were acquired on the NIST campus in Gaithersburg, MD. The results imply that it is possible to achieve 0.5% and lower Type A uncertainties in reflectance measurements with near simultaneous measurements of a region of interest and a reference target such as a standard reflectance panel. The CoV of the ratio between two measurements will be related to the atmospheric conditions, *e.g.* ozone and water vapor concentrations and the strength of turbulence along the measurement path.

Parameterizing *in situ* correlations at a vicarious calibration site may impact protocols for times between measurements of a ground target and associated reflectance panel. If implemented in vicarious calibration site mapping, the reduction in Type A uncertainties for measurements taken contemporaneously will reduce a satellite sensor's vicarious calibration uncertainty budget, enabling vicarious calibration of the sensor with fewer measurements than are currently required.

**\*Disclaimer.** Certain commercial equipment, instruments, or materials are identified in this paper in order to specify the experimental procedure adequately. Such identification is not intended

to imply recommendation or endorsement by the National Institute of Standards and Technology, nor is it intended to imply that the materials or equipment identified are necessarily the best available for the purpose.

**Author Contributions:** Conceptualization, SW Brown and DW Allen; methodology, SW Brown.; software, SW Brown and MA Litorja; validation, DW Allen and JK Marrs; formal analysis, SW Brown; investigation, SW Brown and DW Allen; data curation, SW Brown; writing—original draft preparation, SW Brown; writing—review and editing, SW Brown, DW Allen and JK Marrs. All authors have read and agreed to the published version of the manuscript.

**Data Availability Statement:** This section will be filled in following acceptance of the manuscript for publication.

**Acknowledgments:** We would like to thank Michael Feinholz and Mark Yarbrough, Moss Landing Marine Laboratories, San Jose State University, for the generous loan of the multiple fiber spectrograph used in this work. We would also like to thank Dr. B. Carol Johnson, NIST, for productive input on the framework of the manuscript.

**Conflicts of Interest:** The authors declare no conflicts of interest.

## Abbreviations

The following abbreviations are used in this manuscript:

COV            Coefficient of Variation  
MIFC          Multiple-Input Fiber-Coupled  
MLML        Moss Landing Marine Laboratories  
RadCalNet   Radiometric Calibration Network  
VIIRS        Visible Infrared Imaging Radiometer Suite

## References

1. Johnson, B.C., Personal Communication.
2. EROS Cal/Val Center of Excellence (ECCOE) Test Sites Catalog.
3. CEOS Vicarious Calibration. Available from: [https://calvalportal.ceos.org/cal/val-wiki/-/wiki/CalVal+Wiki/Vicarious+Calibration/pop\\_up](https://calvalportal.ceos.org/cal/val-wiki/-/wiki/CalVal+Wiki/Vicarious+Calibration/pop_up).
4. University of Arizona Remote Sensing Group Sensor Calibration. Available from: <https://wp.optics.arizona.edu/rsg/research/general-2/sensor-calibration/>.
5. Bouvet, M., et al., RadCalNet: A Radiometric Calibration Network for Earth Observing Imagers Operating in the Visible to Shortwave Infrared Spectral Range. *Remote Sensing*, 2019. 11(20): p. 2401.
6. Tuli, F.T.Z., et al., New Approach for Temporal Stability Evaluation of Pseudo-Invariant Calibration Sites (PICS). *Remote Sensing*, 2019. 11(12): p. 1502.
7. Shrestha, M., et al., Extended Pseudo Invariant Calibration Sites (EPICS) for the Cross-Calibration of Optical Satellite Sensors. *Remote Sensing*, 2019. 11(14): p. 1676.
8. Choi, T., et al., Chapter 15 - On-orbit VIIRS sensor calibration and validation in reflective solar bands (RSB), in *Field Measurements for Passive Environmental Remote Sensing*, N.R. Nalli, Editor. 2023, Elsevier. p. 263–280.
9. University of Arizona Spaceborne/Airborne Sensor Calibration. Available from: <https://wp.optics.arizona.edu/rsg/research/general-2/sensor-calibration/>.
10. Zibordi, G., et al., System Vicarious Calibration for Climate and Global Long-Term Operational Ocean Color Applications. *Bulletin of the American Meteorological Society*, 2025. 106(2): p. E394–E407.
11. Thome, K. Railroad Valley Playa for use in vicarious calibration of large footprint sensors. Available from: [https://calvalportal.ceos.org/documents/10136/18915/Railroad+Valley+Playa+for+use+in\\_thome.pdf/eca25535-c34f-4d75-9822-bc17f91f6de1](https://calvalportal.ceos.org/documents/10136/18915/Railroad+Valley+Playa+for+use+in_thome.pdf/eca25535-c34f-4d75-9822-bc17f91f6de1).

12. Thome, K.J., Absolute radiometric calibration of Landsat 7 ETM+ using the reflectance-based method. *Remote Sensing of Environment*, 2001. 78(1): p. 27–38.
13. Ong, C., et al., Reflectance-Based Imaging Spectrometer Error Budget Field Practicum at the Railroad Valley Test Site, Nevada [Technical Committees]. *IEEE Geoscience and Remote Sensing Magazine*, 2018. 6(3): p. 111–115.
14. Czapla-Myers, J.S., et al., The Ground-Based Absolute Radiometric Calibration of the Landsat 9 Operational Land Imager. *Remote Sensing*, 2024. 16(6): p. 1101.
15. Kunkel, K.E., D.L. Walters, and G.A. Ely, Behaviour of the Temperature Structure Parameter in a Desert Basin. *Journal of Applied Meteorology*, 1981. 20: p. 130–136.
16. Christakos, G., Chapter X - Special Classes of Spatiotemporal Random Fields, in *Spatiotemporal Random Fields (Second Edition)*, G. Christakos, Editor. 2017, Elsevier. p. 383–408.
17. Clark, D.K., et al., MOBY, a radiometric buoy for performance monitoring and vicarious calibration of satellite ocean color sensors: Measurements and data analysis protocols, in *Ocean Optics Protocols for Satellite Ocean Color Sensor Validation*, rev. 4. 2003: Greenbelt, MD, NASA Goddard Space Flight Center.
18. Boss, A. Ocean Color System Gets a 'Refresh,' Allowing for More Precise and Accurate Measurements. 2023; Available from: <https://www.nist.gov/news-events/news/2023/01/ocean-color-system-gets-refresh-allowing-more-precise-and-accurate>.
19. Yarbrough, M., et al., Simultaneous measurement of up-welling spectral radiance using a fiber-coupled CCD spectrograph. *Optical Engineering + Applications*. Vol. 6680. 2007: SPIE.
20. Franz, B.A., et al., Sensor-independent approach to the vicarious calibration of satellite ocean color radiometry. *Applied Optics*, 2007. 46(22): p. 5068–5082.
21. Moss Landing Marine Laboratories. Available from: <https://mlml.sjsu.edu/>.
22. Houston, J.M., C.J. Zarobila, and H.W. Yoon, Achievement of 0.005% combined transfer uncertainties in the NIST detector calibration facility. *Metrologia*, 2022. 59(2): p. 025001.

**Disclaimer/Publisher's Note:** The statements, opinions and data contained in all publications are solely those of the individual author(s) and contributor(s) and not of MDPI and/or the editor(s). MDPI and/or the editor(s) disclaim responsibility for any injury to people or property resulting from any ideas, methods, instructions or products referred to in the content.